



Contents lists available at ScienceDirect

Physica D

journal homepage: [www.elsevier.com/locate/physd](http://www.elsevier.com/locate/physd)

# Localized states and non-variational Ising–Bloch transition of a parametrically driven easy-plane ferromagnetic wire

Marcel G. Clerc<sup>a</sup>, Saliya Coulibaly<sup>a,b,\*</sup>, David Laroze<sup>c</sup>

<sup>a</sup> Departamento de Física, Facultad de Ciencias Físicas y Matemáticas, Universidad de Chile, Casilla 487-3, Santiago, Chile

<sup>b</sup> Laboratoire de Cristallographie et Physique Moléculaire (LACPM), UFR Sciences des Structures de la Matière et Technologies (UFR SSMT), Université de Cocody, Abidjan, Cote d'Ivoire

<sup>c</sup> Instituto de Alta Investigación, Universidad de Tarapacá, Casilla 7D, Arica, Chile

## ARTICLE INFO

### Article history:

Received 19 November 2008

Received in revised form

6 October 2009

Accepted 8 October 2009

Available online 14 October 2009

Communicated by J. Bronski

### PACS:

45.70.Qj

47.54.+r

05.45.-a

### Keywords:

Landau–Lifshitz–Gilbert equation

Nonlinear forced oscillator

Localized states

Parametrically driven damped nonlinear

Schrödinger equation

## ABSTRACT

A time-periodic magnetic field applied transversally to the hard axis of an extended easy-plane ferromagnetic sample can produce parametric resonance. For the 2:1 resonance, the prototype order-parameter-equation derived from the Landau–Lifshitz–Gilbert dynamical model for the precessional motion is the parametrically driven damped nonlinear Schrödinger equation. Unfortunately this standard approximation fails to meet the stability feature of the synchronized precession states, and we propose some amendment. Localized solutions supported by the uniform states are characterized and classified into two types: motionless and propagative states, rising through a non-variational Ising–Bloch transition. We propose and investigate a dynamical model ruling this transition.

© 2009 Elsevier B.V. All rights reserved.

## 1. Introduction

Macroscopic particle type solutions or localized states in non-equilibrium systems have been observed in different fields, such as: domains in magnetic materials [1], chiral bubbles in liquid crystals [2], current filaments in gas discharges [3], spots in chemical reactions [4], localized states in fluid surfaces waves [5], oscillons in granular media [6,7], isolated states in thermal convection [8,9], solitary waves in nonlinear optics [10–12], among others. These localized states appear as the result of the collective behavior of a large quantity of microscopic components – typically of the order of the Avogadro number – which are described by a few order parameters: position, thickness and so forth [13]. In general, the study of such pattern forming processes is strongly related to the possibility of obtaining the intrinsic evolution of the system under study in the form of a small set of equations for some gross variables or order of parameters: the amplitude equations. This reduction is possible due to a separation of time scales, which allows a description in terms of the slowly varying variables. Indeed, these variables are fluctuating variables due to the elimination of a large number of rapidly evolving degrees of freedom whose effect can be modeled including suitable stochastic terms in the amplitude equations. One has a large variety of amplitude equations depending on both the spatial and the spatio-temporal dynamics of the original system under consideration [14].

Usually non-equilibrium systems are maintained out of equilibrium by means of an external forcing, which can be constant or time-dependent. In the case of time-dependent forcing one can identify two mechanisms: the direct injection of energy into the system or the modulation of at least one parameter of the system under study. This second type of energy injection is often denominated parametric forcing. In practice, for a parametrically driven oscillator, resonance occurs at a frequency, which is different from the forcing. This is the

\* Corresponding author at: Departamento de Física, Facultad de Ciencias Físicas y Matemáticas, Universidad de Chile, Casilla 487-3, Santiago, Chile. Tel.: +56 29784342; fax: +56 26790148.

E-mail address: [saliya@dfi.uchile.cl](mailto:saliya@dfi.uchile.cl) (S. Coulibaly).

characteristic feature of a parametrically driven system. Faraday or subharmonic waves [15,16], where the system responds at half of the driving frequency, constitute one of the most known examples. Parametric excitation of localized structures in extended systems is a topic of considerable interest in several fields of physics, including fluid dynamics [17–22], ferromagnetism and anti-ferromagnetism [23,24], nonlinear optics [25–27] and liquid crystals [28]. We recall that localized structures can be used as information carriers in nonlinear optics [29].

A very general representative model used to study parametrically forced systems including dissipative effects is the parametrically driven damped nonlinear Schrödinger equation (PDNLS). We refer to this procedure as the Standard approach. This model predicts interesting behaviors and has a large variety of solutions such as dissipative solitons below and close to the parametric resonance or above, and it also presents Faraday instability or modulational instability [16,30–37]. In addition, the PDNLS equation has two symmetrical uniform states inside the first Arnold's tongue.

In systems presenting these kinds of stable symmetrical states, the existence of a wide family of inhomogeneous solutions has been shown [38]. These states are called localized structures. Indeed, these localized states are described by two parameters, their position and their thickness. The thickness is proportional to a multiple of the characteristic length of the spatially damped oscillations appearing in the domain wall or kink solution of the considered family. Hence, these types of localized states can be obtained as a superposition of domain walls. Recently, we have shown that parametrically driven dissipative systems exhibit these types of localized states [39]. However, the PDNLS model does not account for these states.

On the other hand, the interaction of different states is characterized by fronts, domain walls or defects, which are interfaces between different extended steady states [40]. For example, bistable systems can exhibit fronts connecting two homogeneous states. The features and dynamics of such domain walls have attracted attention in different areas of science, including biology, chemistry and physics [41]. Generically, a front connecting two different uniform states moves in such a way that the more stable state invades the other one [42,43].

In the case of one- or two-dimensional gradient or variational systems, the front velocity of a flat interface is proportional to the energy difference between the two asymptotic states. This velocity can be modified by the curvature of the front, according to the Gibbs–Thomson effect [44]. Changing parameters, the metastable state – less stable state – becomes energetically equivalent to the other state, thus the front stops propagating; in particular, when the system is at the Maxwell point [45]. Increasing further the control parameter, the propagation direction is reversed; that is, the most energetically favored state invades the less favored one. The previously mentioned scenarios change drastically, when one considers a system with discrete symmetry, for instance reflection symmetry. The domain walls connecting such states are generically at rest as consequence of the discrete symmetry. Both states are “energetically” equivalent. However, under spontaneous symmetry-breaking these fronts can support a nonzero asymptotic speed. A classical example of such a phenomenon is the so-called Ising–Bloch Transition [46] observed in ferromagnets [47], liquid crystal [48], and chemical reactions [49]. Gradient or variational systems do not exhibit this phenomenon, since the front speed is proportional to the energy difference between these equivalent states. The dynamics of non-gradient systems always can be decomposed in two parts, a dissipative and a remnant; such that a Lyapunov functional – *Non-equilibrium potential* – characterizes the dissipative dynamics [50,51]. The uniform steady states of non-equilibrium systems minimize the non-equilibrium potential and the remnant dynamics is responsible of non-trivial dynamics like oscillations, chaos and so forth. Therefore, the front propagation in the non-equilibrium Ising–Bloch transition is a consequence of remnant dynamics [52]. Due to the universal nature of walls propagation linking equivalent states, the transition between static and moving fronts is usually denominated non-variational or non-equilibrium Ising–Bloch transition [53].

The aim of this paper is to study the formation and the dynamics of localized particle type solutions inside the first Arnold's tongue of a parametrically driven dissipative system. For this purpose, we consider as prototype system an easy-plane ferromagnetic spin chain in the presence of both a constant and a time-periodic external magnetic field perpendicular to the hard axis, by means of the Landau–Lifshitz–Gilbert (LLG) equation. We refer to these localized structures as localized precession states observed in the forced magnetic wire. We show that the parametrically driven damped nonlinear Schrödinger equation model fails to describe these localized synchronized precession states. We propose a correction of this standard approach, by adding higher order terms. Thus we recover the rich dynamics observed numerically in a forced magnetic wire. Also, we show that these localized precession states can be classified into two types: motionless and propagative states. The transition between motionless and propagative localized states is mediated by a non-variational Ising–Bloch transition.

The manuscript is organized as follows: In Section 2, we present the theoretical model and show that the Landau–Lifshitz–Gilbert equation is equivalent to a nonlinear oscillator. In Section 3, we show that in the quasi-reversible limit, the nonlinear oscillator can be approximated by the parametrically driven damped nonlinear Schrödinger equation. In Section 3, we show that the previous standard approach is structurally unstable. Amending the parametrically driven damped nonlinear Schrödinger equation with higher order terms allows us to understand the dynamics exhibited by the forced magnetic wire. In Section 4, we study this amended model. Section 5 is devoted to the study of the transition between a motionless and a moving wall, which is characterized by a non-variational Ising–Bloch transition. Finally, conclusions are presented in Section 6.

## 2. Parametrically forced magnetic wire

Let us consider a one-dimensional anisotropic Heisenberg ferromagnetic chain formed by  $N$  spins subject to an external magnetic field. The direction of the chain is described by the  $z$ -coordinate,  $\hat{z} \equiv (0, 0, 1)$ , and the external magnetic field is orthogonal to this direction, denoted by  $\hat{x} \equiv (1, 0, 0)$ . Fig. 1 depicts the setup of the system under study. Therefore, the Hamiltonian of the chain reads [54,55]:

$$\mathcal{H} = -J \sum_{i=1}^N \mathbf{S}_i \mathbf{S}_{i+1} + 2D \sum_{i=1}^N (S_i^z)^2 - g\mu H_x \sum_{i=1}^N S_i^x, \quad (1)$$

where  $J$  is the exchange coupling constant,  $H_x$  and  $D$  stand for the external magnetic field and the anisotropy energy, respectively. When the quantum effects are small enough, the spin vectors  $\mathbf{S}_i$  can be treated as a classical spin or a magnetic moment [56]. According to this last assumption, the dynamics of the magnetic moment  $\mathbf{S}_i$  is governed by  $\dot{\mathbf{S}}_i = -\gamma \mathbf{S}_i \times (\partial \mathcal{H} / \partial \mathbf{S}_i)$  [57], where  $\gamma$  is the gyromagnetic constant.

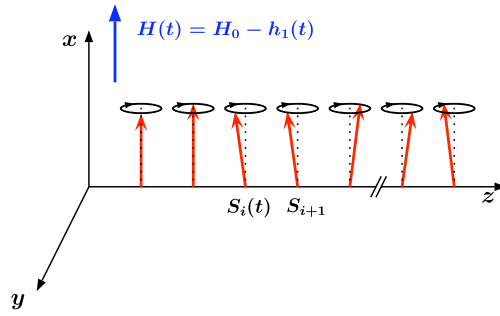


Fig. 1. Schematic representation of the spin chain modeled by the Hamiltonian (1).

Hence  $\mathbf{S}_i$  satisfies

$$\dot{\mathbf{S}}_i = -\gamma \mathbf{S}_i \times \left[ -J (\mathbf{S}_{i-1} - 2\mathbf{S}_i + \mathbf{S}_{i+1}) + 4D S_i^z \hat{z} - g\mu H_x \hat{x} + 2J \mathbf{S}_i \right]. \quad (2)$$

To study the continuum limit of this set of the ordinary differential equations, we can assume that:

$$\mathbf{S}_i(t) \rightarrow \mathbf{S}(z, t) \quad \text{and} \quad (3a)$$

$$\frac{J dz^2}{\gamma^{-1}} \left( \frac{\mathbf{S}_{i+1} - 2\mathbf{S}_i + \mathbf{S}_{i-1}}{dz^2} \right) \rightarrow l_{ex} \partial_z^2 \mathbf{S}(z, t), \quad (3b)$$

where  $l_{ex}$  denotes the characteristic interaction length. Moreover, introducing phenomenologically the Gilbert damping, the motion of the magnetization field is governed by the well-known Landau–Lifshitz–Gilbert (LLG) equation:

$$\partial_\tau \mathbf{M} = \mathbf{M} \times \left[ \mathbf{M}_{zz} - \beta (\mathbf{M} \cdot \hat{z}) \hat{z} + \mathbf{H}_e - \alpha \partial_\tau \mathbf{M} \right], \quad (4)$$

where  $\mathbf{M}$  stands for the unit vector of the magnetization. We have also introduced the following normalization  $\{\tau \rightarrow \gamma M_s t, \beta \rightarrow 4D/\gamma, \mathbf{H}_e \rightarrow g\mu \mathbf{H}/\gamma M_s\}$  with  $M_s$  the magnetization of saturation defined as  $\mathbf{M} = \mathbf{S}/M_s$ ; where  $\beta > 0$  is the anisotropy constant (easy-plane magnetization), and  $\alpha$  is the damping parameter. For several types of magnetic materials, this parameter is small. When the magnetic field is time-dependent, the above model (4) is a time reversible system perturbed with injection and dissipation of energy, i.e. a quasi-reversible system, as long as these perturbations remain small. The instabilities of these types of systems have been studied during the last decades [58].

### 2.1. Parametric resonance in an easy-plane ferromagnetic wire

For the configuration under study, the stable steady state of the chain ( $\mathbf{M}_0$ ) corresponds to all the spins or magnetic moments parallel to the external magnetic field, that is  $\mathbf{M}_0 \equiv (1, 0, 0) = \hat{x}$ . Hence, the motion of the magnetization is described by the angular deviation with respect to the vertical position  $\hat{x}$ . In this case, according to the magnetization conservation condition we have  $m_x = \sqrt{1 - (m_y^2 + m_z^2)}$ . Then, for the small deviations, the component along the  $\hat{x}$ -axis can be expressed as:

$$m_x \simeq 1 - \frac{m_y^2 + m_z^2}{2} + O(m_y^4, m_z^4). \quad (5)$$

Therefore, using the standard nonlinear method [14] the system reads:

$$\begin{aligned} \dot{m}_y &= (\beta + H) m_z - \partial_z^2 m_z - \alpha H m_y - \frac{\beta}{2} (m_y^2 + m_z^2) m_z, \\ \dot{m}_z &= -H m_y + \partial_z^2 m_y - \alpha (\beta + H) m_z. \end{aligned} \quad (6)$$

For a constant external applied magnetic field ( $\mathbf{H}_e \equiv H_0$ ), the temporal linear stability analysis of the basic state  $\mathbf{M}_0$  with respect to a homogeneous perturbation of the form  $\delta m_j e^{\sigma t}$  ( $j = \{y, z\}$  and  $\delta m_j \ll 1$ ) [14], leads in the limit of a weak Gilbert damping to two eigenvalues of the form

$$\sigma_\pm \simeq -\mu \pm i\omega_0.$$

Here  $\mu$  and  $\omega_0$  are respectively the effective damping and the angular velocity of the gyromagnetic precession. They have the explicit form:

$$\mu = \left( H_0 + \frac{\beta}{2} \right) \alpha, \quad (7a)$$

$$\omega_0 = \sqrt{H_0 (\beta + H_0)}. \quad (7b)$$

That is, the vertical state is the only stable state for all the magnetic moments of the chain. Any perturbation to this solution will decrease exponentially with the characteristic decay rate  $\tau = 2/\alpha (\beta + 2H_0)$  as illustrated in Fig. 2.

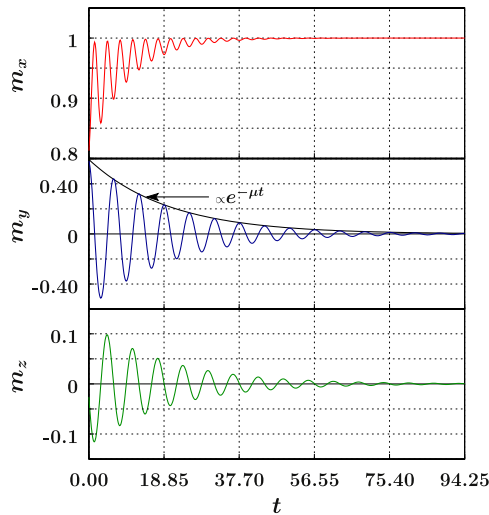


**Fig. 2.** Temporal evolution at an arbitrary position in the ferromagnetic spin chain, resulting of the numerical simulation of the model (4) with a constant external field ( $H_0 = 0.20$ ) for  $\beta = 4.80$ ,  $\alpha = 0.02$  in dimensionless units. For these specific values the angular velocity is  $\omega_0 = 1.00$  and the decay rate of the envelop for a small perturbation (solid black line) is  $\lambda = 0.05$ .

The above scenario changes drastically when the external field is a time-dependent function with both constant and time-periodic components, that is,  $\mathbf{H}_e = [H_0 - h_1(t)]\hat{x} = (H_0 - h \sin \Omega t)\hat{x}$ . Thus, rewriting Eq. (6) for one of the components, for instance  $m_z$ , after some calculations one can obtain in the weakly nonlinear regime (quasi-reversible extended oscillator):

$$\ddot{m}_z = -\omega_0^2 m_z + (\beta + 2H_0) \partial_z^2 m_z - \mu \dot{m}_z - \frac{\dot{h}_1}{H_0} \dot{m}_z + (\beta + 2H_0) h_1 m_z + \frac{\beta H(t)}{2} (m_y^2 + m_z^2) m_z. \quad (8)$$

The component  $m_y$  is related to  $m_z$  by

$$m_y \approx -\frac{1}{H(t)} \dot{m}_z \approx \frac{1}{H_0} \left( 1 + \frac{1}{H_0} h_1(t) \right) \dot{m}_z. \quad (9)$$

Eq. (8) is a forced nonlinear extended oscillator, which has as steady state  $\mathbf{M}_0$ . It is well known that this type of oscillator exhibits a parametric resonance, that is, a resonance that occurs when the forcing frequency is close to twice the natural frequency of the system—2:1 resonance [59]. The dynamics around the trivial state  $m_z = 0$  of model (8) is characterized by a linear operator with time-periodic coefficients. Close to the parametric resonance ( $\Omega \approx 2\omega_0$ ), we can use the Ansatz  $m_z = \Re(Ae^{(\sigma_p + i\omega_0)t})$ , which is motivated by the Floquet method, obtaining

$$\sigma_{p\pm} = -\mu + \sqrt{\gamma^2 - \nu^2} \pm i\nu, \quad (10)$$

where

$$\gamma \equiv \frac{\beta h}{4\omega_0}, \quad (11a)$$

$$\nu \equiv \frac{\Omega}{2} - \omega_0. \quad (11b)$$

The quantities  $\{\gamma, \nu\}$  are respectively the effective driving strength and the detuning parameter. Hence, following (10), a small perturbation of the trivial state decreases exponentially when  $\gamma^2 < \mu^2 + \nu^2$  and increases exponentially when  $\gamma^2 > \mu^2 + \nu^2$ . A perturbation in this region leads to an undamped precession with a finite angular deviation determined by the nonlinear saturation. This process is depicted in Fig. 3. Hence, the marginal curve  $\gamma^2 = \mu^2 + \nu^2$  characterizes the stability of the vertical state  $\mathbf{M}_0$ , which is the so-called Arnold's tongue. Fig. 4 illustrates Arnold's tongue and region (III).

Neglecting the spatial dependence in model (8), we observe numerically for negative detuning the existence of four nonzero homogeneous states, two stable and two unstable. These states appear by a saddle-node bifurcation at  $\gamma = \mu$ , and  $\nu < 0$  and two of them – the unstable ones – disappear by an inverted pitchfork bifurcation at Arnold's tongue. In Fig. 4 this region is represented by (I), then in this area we have coexistence between the nonprecessing state (vertical solution) and the other nonzero states (bistability region). The trivial state  $m_z = 0$  is stable in the regions  $\{(0), (I), (II)\}$  represented in Fig. 4.

### 3. The parametrically driven nonlinear Schödinger equation as an approximation of the LLG model

The inclusion of the spatial coupling modifies the bifurcation diagram of the above scenario, because generically the spatial instability anticipates the homogeneous one. Additionally as it is depicted in Fig. 3, in the long time limit, the dynamics is ruled by the nonlinearities. Hence, these effects must be included in order to have an appropriate description of the forced magnetic wire. However, the model (4) is complex enough to figure out the spatio-temporal dynamics which it can exhibit. For this purpose, we shall study the dynamics close to the quasi-reversible parametric resonance, that is, we consider the quasi-reversible nonlinear oscillator (8), since it is a good description of the three coupled basic equations in the limit of small injection and dissipation of energy:  $h \sim \alpha \ll H_0$ .

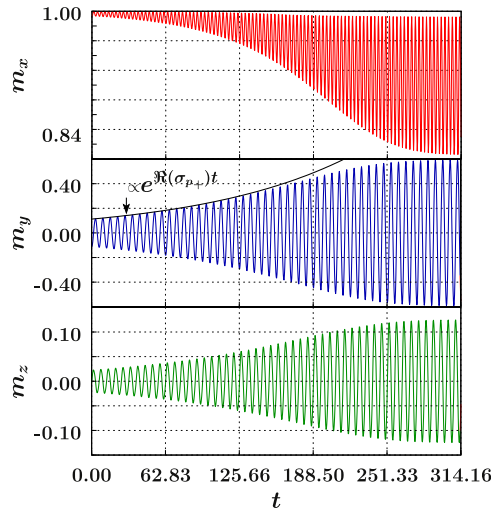


**Fig. 3.** Temporal evolution at an arbitrary position in the ferromagnetic spin chain, resulting on the numerical simulation of model (4) with an external field exhibiting both constant and time-periodic component with frequency  $\Omega = 2\omega_0$ . The parameters are the same used in figure Fig. 2, where in addition we have here  $\nu = 0.00$  and  $h = 0.05$ . The linear growth rate  $\Re(\sigma_{p+}) = 0.008$  corresponds to the predicted value given by the linear stability analysis.

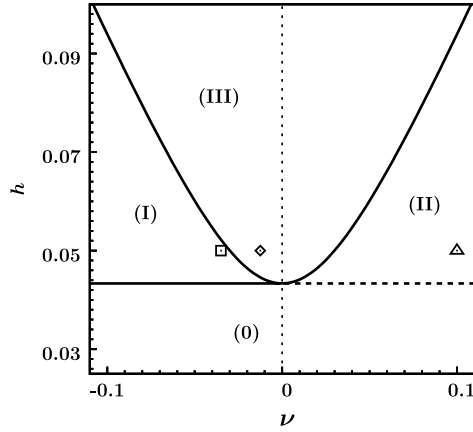


**Fig. 4.** Bifurcation diagram of the parametrically driven LLG Eq. (4), for  $\alpha = 0.02$ ,  $\beta = 4.8$ ,  $H_0 = 0.2$  and  $h = 0.05$ . The solid lines give the edge of Arnold's tongue (III) and the bistability region (I). Faraday instability is represented by horizontal dotted line. The symbols  $\square$ ,  $\diamond$ ,  $\triangle$  correspond to  $\nu = -0.012$ ,  $-0.035$ ,  $0.100$  respectively.

### 3.1. The standard approach for a parametrically forced magnetic wire

We introduce the following Ansatz,

$$m_z = 4 \sqrt{\frac{\omega_0 H_0}{\beta (\omega_0^2 + 3H_0^2)}} \Re(A e^{i(\omega_0 + \nu)t}) + w(x, t, A), \quad (12)$$

in Eq. (8), where  $w(x, t, A)$  is a small correction. Linearizing in  $w(x, t, A)$ , one obtains the following solvability condition (Fredholm alternative) [60] for the amplitude of the oscillations (parametrically driven damped nonlinear Schrödinger equation)

$$\partial_t A = -i\nu A - i|A|^2 A - i\partial_{ZZ} A - \mu A + \gamma \bar{A}, \quad (13)$$

where  $Z \equiv \sqrt{2\omega_0 / (\beta + 2H_0)} z$ . The terms proportional to  $\{\nu, \gamma, \mu\}$  stand for the detuning, effective driving and damping. The nonlinear term and the spatial derivative account for the nonlinear response in frequency and for the dispersion, respectively. Model (13) is a unified description of the envelope evolution of a nonlinear parametrically driven oscillator, when the parameters which determine the temporal and the spatial variation scale as  $\gamma \sim \nu \sim \mu \ll 1$ ,  $\partial_t \sim \nu$ ,  $\partial_z \sim \nu^{1/2}$  and  $|A| \sim \nu^{1/2}$ . Hence, the above solvability condition is of order  $\nu^{3/2}$ . For the extreme limit  $\nu = \gamma = 0$ , the above model is the well-known Nonlinear Schrödinger Equation, which is a Hamiltonian and time reversible model [61].

Eq. (13), known as the parametrically driven damped nonlinear Schrödinger equation, has been intensively used to describe patterns and solitons in several systems such as: vertically oscillating fluid layers [16], localized structures in nonlinear lattices [30], light pulses in optical fibers [31], and the Kerr type optical parametric oscillators [32,36]. Therefore, the LLG equation is expected to exhibit spatially extended and/or localized solutions.

So far the most well known are the dissipative solitons [23] and the modulational instability [62]. Dissipative solitons (see Fig. 5a) are spatially localized exact solutions of the PDNLS and they appear through a saddle–node bifurcation for negative detuning at  $\gamma = \mu$ . These states become unstable at  $\gamma^2 = \mu^2 + \nu^2$  (region I of Fig. 4). In contrast, the modulational instability rises for positive detuning ( $\nu > 0$ )

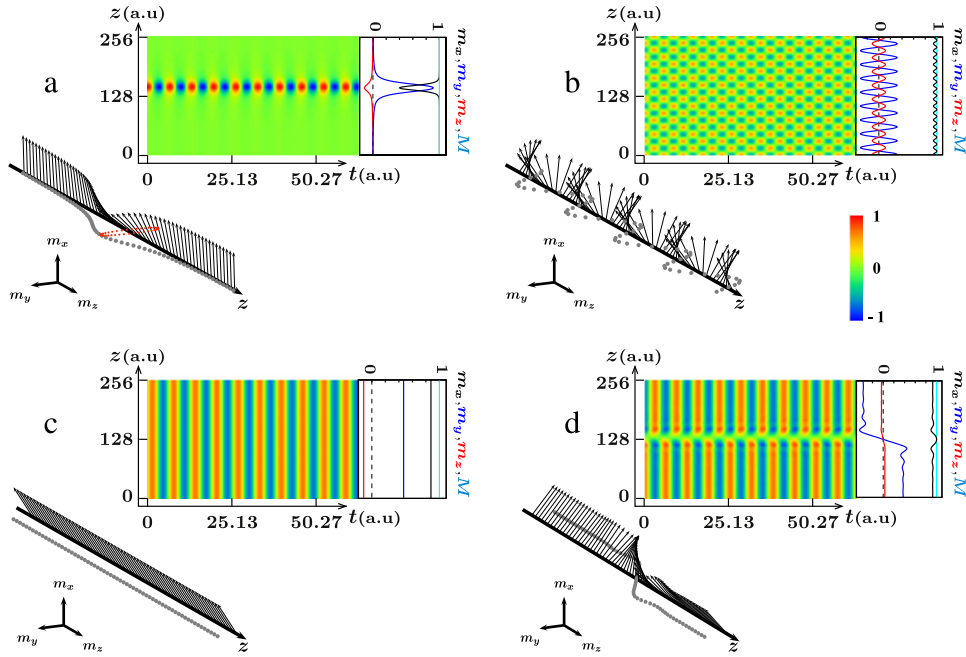


**Fig. 5.** States given by the numerical integration of the LLG model (4) closed to the tip of Arnold's tongue for  $\alpha = 0.02$ ,  $\beta = 4.8$ ,  $H_0 = 0.2$ ,  $h = 0.05$  and detuning [(a)  $\nu = -0.035$ , (b)  $\nu = 0.100$ , (c)  $\nu = -0.012$ , (d)  $\nu = -0.012$ ].

by means of a supercritical bifurcation at  $\gamma = \mu$  and the amplitude is proportional to  $(\gamma - \mu)^{1/4}$  [62]. In regions II and III of Fig. 4, we observe numerically pattern states of PDNLS that corresponds to a subharmonic precession wave along the magnetic wire. Fig. 5b shows the spatio-temporal diagram of the standing wave and its inset depicts the patterns observed at a given time. The wave number of this wave at the onset of the spatial bifurcation is  $k_c = \pm\sqrt{\nu}$ .

On the other hand the uniform states, which correspond to a synchronized precession of all the spins of the chain, is depicted in Fig. 5c. These solutions correspond to homogeneous steady states of the PDNLSE  $A(x, t) = A_{0\pm} \equiv R_{0\pm} e^{i\varphi_0}$  with

$$R_{0\pm} = \sqrt{-\nu \pm \sqrt{\gamma^2 - \mu^2}}, \quad (14a)$$

$$\varphi_0 = \frac{1}{2} \arccos\left(\frac{\mu}{\gamma}\right), \quad (14b)$$

The solutions  $A_{0-}$  and  $A_{0+}$  exist, respectively, in the regions (I) and (I)–(III) depicted in Fig. 4. As a result of the parity symmetry  $A \rightarrow -A$  of Eq. (13), associated with  $(m_x, m_y, m_z) \rightarrow (m_x, -m_y, -m_z)$  of the LLG equation, the system has two solutions which are out of phase. Hence, we expect the existence of stable trajectories that asymptotically connect these two symmetrical states. Numerical simulations of the LLG model show the appearance of these types of solutions, which are usually denominated kink or domain wall solutions. Fig. 5d shows the spatio-temporal dynamics of a kink solution and it represents the domain wall at a given time. As it is illustrated in this figure, the kink solution exhibits damped spatial oscillations with a characteristic length, which converges asymptotically to the states  $R_{0+}$  or  $R_{0-}$ . Accordingly, we can assert that the necessary condition of the existence of these stable kink solutions is the stability feature of the uniform states, which support this domain wall.

### 3.2. The synchronized precession state

Numerically, we have observed uniform stable precession states of LLG only inside Arnold's tongue. We will focus first on this parameter region. In order to determine the stability domain of this solution of the LLG model, we shall use the simplified model (13). For this purpose we introduce the variables  $A(x, t) = r(x, t) e^{i\varphi(x, t)}$ , where  $r(x, t)$  and  $\varphi(x, t)$  are the modulus and the phase field respectively. By substituting this expression in Eq. (13) we obtain

$$\begin{aligned} r_t &= r\gamma \cos 2\varphi - \mu r + 2\partial_z \varphi \partial_z r + r \partial_{zz} \varphi, \\ r\varphi_t &= -\nu r - r^3 - r\gamma \sin 2\varphi - \partial_{zz} r + (\partial_z \varphi)^2 r. \end{aligned} \quad (15)$$

These equations have uniform solutions which are given in formulas (14). For the non-extended dynamical system of the above model – system without spatial dependence – the uniform steady states  $\{R_{0-}, \varphi_0\}$  and  $\{R_{0+}, \varphi_0\}$  are unstable and stable respectively. In order to study the stability features of the state  $\{R_{0+}, \varphi_0\}$  for the extended model (15), we introduce the Ansatz

$$\begin{aligned} r &= R_{0+} + \rho, \\ \varphi &= \varphi_0 + \theta, \end{aligned}$$

where  $\rho$  and  $\theta$  are small corrections. The linearized system reads

$$\begin{aligned} \rho_t &= -2\gamma R_{0+} \sin(2\varphi_0)\theta + R_{0+} \partial_{zz} \theta, \\ R_{0+} \theta_t &= -\nu \rho - 3R_{0+}^2 \rho - 2\gamma \sin(2\varphi_0)\rho - 2\gamma R_{0+} \cos(2\varphi_0)\theta - \partial_{zz} \rho. \end{aligned} \quad (16)$$

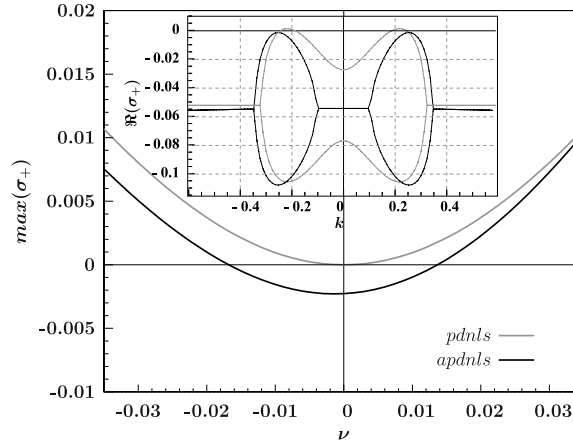


**Fig. 6.** Growth rate of the most unstable wave number  $k_c$  resulting from the linear stability analysis of : the PDNLS (Eq. (13)) (gray line) and the amended PDNLS (Eq. (19)). The inset Figure gives the respective spectra for  $\nu = -0.0125$ ,  $\alpha = 0.02$ ,  $\beta = 4.8$ ,  $H_0 = 0.2$  and  $h = 0.05$ .

Combining the above equations and using the relation  $-(\nu + \gamma \sin 2\varphi_0) R_{0+} - R_{0+}^3 = 0$ , one obtains

$$\theta_{tt} = 4\gamma \sin(2\varphi_0)\theta R_{0+}^2 + 2(\gamma \sin(2\varphi_0) - R_{0+}^2)\theta_{zz} - 2\mu\theta_{\tau} - \theta_{zzzz}. \quad (17)$$

Assuming a perturbation of the form  $\theta = \tilde{\theta}e^{(\sigma t + ikz)}$ , the growth rate  $\sigma$  satisfies the relation

$$(\sigma + \mu)^2 = (\mu^2 + \nu^2) - \left(2R_{0\pm}^2 + \nu - k^2\right)^2. \quad (18)$$

Hence, the solution  $A = R_{0+}e^{i\varphi_0}$  is stable if  $\Re(\sigma) < 0$ , that is,

$$\Re\left(-\mu + \sqrt{\mu^2 + \nu^2 - \left(-\nu - k^2 \pm 2\sqrt{\gamma^2 - \mu^2}\right)^2}\right) < 0.$$

The typical growth rate curve as function of the wave number is depicted by the inset of Fig. 6, which is characterized by two lobes; where the maxima are reached in the highest extreme of the lobes at the critical wave number  $k_c = \pm\sqrt{-\nu + 2\sqrt{\gamma^2 - \mu^2}}$ . The growth rate at this critical wave number is  $\sigma(k_c) = \sigma_c = -\mu + \sqrt{\mu^2 + \nu^2}$ . It is worthy to note that this  $\sigma_c$  is non-negative whatever  $\mu$  and/or  $\nu$ . Thus, inside Arnold's tongue, as shown in Fig. 6, the homogeneous steady state  $A = R_{0+}e^{i\varphi_0}$  is always spatially unstable. Fig. 7 shows the dynamical evolution of the synchronized precession states plus a small perturbation. The synchronized precession state suffers a spatial instability which gives rise to a pattern state with a wave number close to  $k_c$  (cf. Fig. 7b). However, the growth rate curve is marginal ( $\sigma_c = 0$ ) for  $\nu = 0$ , that is, the spectrum satisfies  $\sigma(k) \leq 0$ . Hence, from the point of view of dynamical systems theory, the uniform steady state  $A = R_{0+}e^{i\varphi_0}$  of model (13) is structurally unstable close to zero detuning [63]. That is, any small modification of model (13) can modified the stability features of the nonzero uniform states. The above results, confirmed by numerical integration of the parametrically driven damped nonlinear Schrödinger equation (Fig. 7) are in contradiction with previous observations in the original system (cf. Fig. 5).

Therefore, the dynamical features of the synchronized precession states observed numerically in the Landau–Lifshitz–Gilbert model (4) are not described correctly by the parametrically driven damped nonlinear Schrödinger equation (13). Consequently, this standard amplitude equation cannot describe the wall domains or the localized precession states supported by the uniform precession states [39]. As we have mentioned the parametrically driven damped nonlinear Schrödinger equation is structurally unstable for small detuning, then the inclusion of higher order terms in the amplitude equation can modify the stability features of the homogeneous states under study. Hence, this statement suggests the necessity to amend the standard approach.

#### 4. The amended amplitude equation

To describe the synchronized precession state exhibited by the magnetic forced wire under study, it is required to consider higher order terms in the amplitude equation (13) since these terms can restore the features of the uniform states, in the parameter region where the uniform precession state  $R_{0+}$  is marginal ( $\nu = 0$ ). We expect that any small corrections of the amplitude equation can render this state linearly stable or unstable. When we consider the dominating higher order terms the amplitude equation reads (*amended amplitude equation*)

$$\partial_t A = -i\nu A - (i - c)|A|^2 A - i\partial_z^2 A - \mu A + \gamma(1 + i\Gamma)\bar{A} - \gamma\alpha'|A|^2 \bar{A} - \gamma\delta A^3, \quad (19)$$

where the coefficients  $c$ ,  $\Gamma$ ,  $\alpha'$  and  $\delta$  are deduced in Appendix A (see Eq. (A.13j)). Notice that the extra terms on the right-hand side are of order  $\nu^{5/2}$ . The terms proportional to  $\alpha'$  and  $\delta$  account for nonlinear forcing. In order to study the stability features of the synchronized precession states we shall compute this state and its eigenvalues numerically. Let  $\tilde{A}_{0+} = \tilde{R}_{0+} \exp(i\tilde{\varphi}_0)$  be the synchronized precession state of the amended amplitude equation, the stability analysis around this solution gives the following dispersion relation

$$\tilde{\sigma}_{\pm} = \varsigma_1 \pm \sqrt{\varsigma_2^2 + \varsigma_3^2 - \varsigma_4^2}, \quad (20)$$

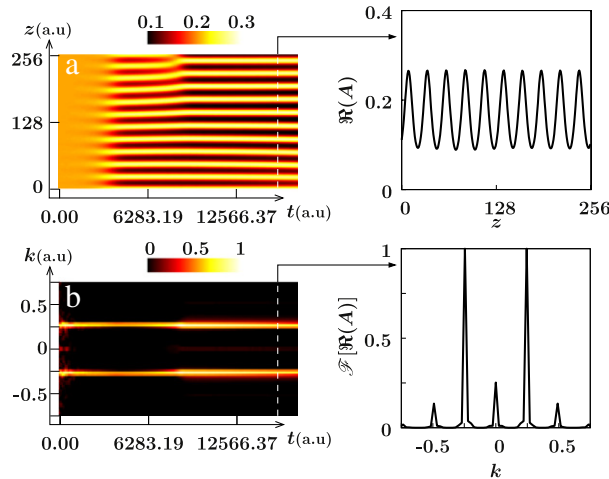


**Fig. 7.** Spatio-temporal evolutions of a small random perturbation of the uniform steady state of Eq. (13) in real (a) and Fourier ( $\mathcal{F}[\cdot]$ ) space (b), for  $\mu = 0.052$ ,  $\gamma = 0.06$ ,  $\nu = -0.0125$ .

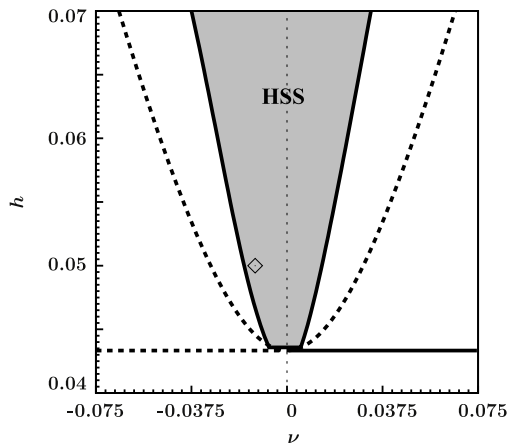


**Fig. 8.** Arnold's tongue of the LLG deduced from the amended amplitude equation (19). The gray region corresponds to the stability domain of the synchronized precession state (HSS). The ( $\diamond$ ) locates the value of the detuning used in Fig. 5c.

with

$$\zeta_1 = -\mu + 2c\tilde{R}_0 - \gamma (\alpha' + 3\delta) \tilde{R}_0^2 \cos(2\tilde{\varphi}), \quad (21a)$$

$$\zeta_2 = \gamma + (c \cos(2\tilde{\varphi}) + \sin(2\tilde{\varphi}) - 2\gamma\alpha') \tilde{R}_0^2, \quad (21b)$$

$$\zeta_3 = \gamma\Gamma - (\cos(2\tilde{\varphi})) - c \sin(2\tilde{\varphi}) \tilde{R}_0^2, \quad (21c)$$

$$\zeta_4 = \nu + 2\tilde{R}_0^2 - k^2 - \gamma (\alpha' - 3\delta) \tilde{R}_0^2 \sin(2\tilde{\varphi}). \quad (21d)$$

The growth rate curve as function of the wave number again is formed by two lobes as it is depicted in Fig. 6. Then the most unstable mode rises with the wave number

$$\tilde{k}_c = \pm \sqrt{\nu + 2\tilde{R}_0^2 - \gamma (\alpha' - 3\delta) \tilde{R}_0^2 \sin(2\tilde{\varphi})}. \quad (22)$$

The growth rate of this mode can be computed numerically; for instance taking the parameters used in Fig. 5c, we obtain the black solid line in Fig. 6. In opposition to the parametrically driven damped nonlinear Schrödinger equation we observe a small range around  $\nu = 0$ , in which the synchronized homogeneous state is stable as consequence of the negative sign of the growth rate. Repeating this operation for different values of the parametric driving amplitude one can determine the stability region of the synchronized homogeneous states inside Arnold's tongue. Fig. 8 shows the stable region for the synchronized homogeneous states.

Since the stability of the synchronized precession states is recovered, the LLG system is expected to exhibit inhomogeneous solutions that asymptotically connect the synchronized precession state with itself – *localized state* – or with the other one which is out of phase – *kink state*. This last extended state and its parity reflected image – *anti-kink* – appear to be the simplest particle type solution. It is important to note that in one-dimension their interactions give the main tool to understand the formation process of localized states [38,64,65]. It leads to describe the localized states through the size of them, which appears to be roughly a multiple of the characteristic length of the damped spatial oscillations present in the kink state (see Fig. 5). Fig. 9 depicts the family of localized states, which present some of the localized precession states exhibited by the LLG equation. The calculated wave number using the proportionality between the

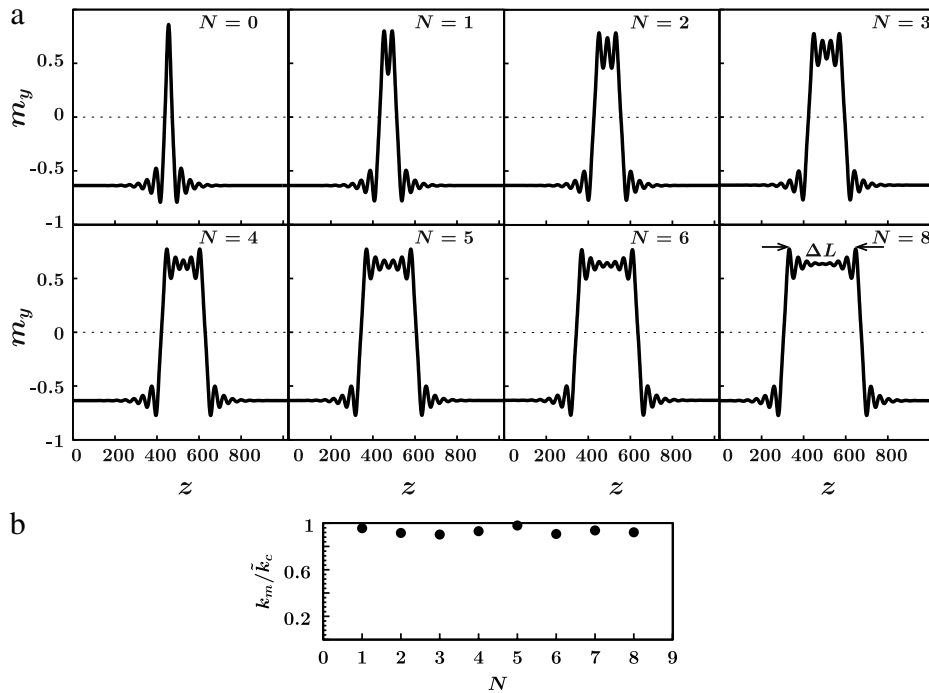


**Fig. 9.** Non-exhaustive particle type solutions (a) exhibited by the LLG model for the same parameters used in Fig. 5c. The distance  $\Delta L$ , giving the size of the localized state, was shown to be a multiple of the wave length of the damped spatial oscillations.  $N$  corresponds to the number of spatial periods inside  $\Delta L$ . The calculated wave number  $k_m = \frac{2\pi N}{\Delta L}$  appears as a constant variable. The average  $\langle k_m \rangle = 0.161$  is closed to the predicted value  $k_c = 0.173$ .

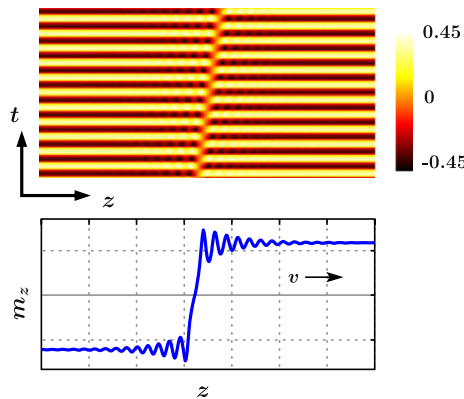


**Fig. 10.** Bloch type wall exhibited by Landau–Lifshitz–Gilbert equation (4), with  $\beta = 6$ ,  $H_0 = 1.125$ ,  $h_0 = 0.775$ ,  $\omega = 2(\sqrt{H_0(H_0 + \beta)} + v)$ ,  $v = -0.05$  and  $\alpha = 0.09$ . The upper picture is a density plot of spatio-temporal dynamics of  $M_z$ .

size and the wave length of the most unstable mode. Compared to predicted one (22) present a relative error of 7% (cf. Fig. 9b). Hence, the amended amplitude equation (19) recovers the rich dynamics exhibited by the parametrically driven magnetic wire.

A ferromagnetic wire exposed to a transversal-periodic external magnetic field is analogue to an extended driven nonlinear oscillator. The standard approach (PDNLS) of such kinds of systems fails to describe an intriguing and infinite family of particle type solutions observed in the original system. According to the theory of dynamical systems, we have amended the structurally unstable standard prototype model and recovered the stability of the synchronized precession states of the parametrically driven magnetic wire. The above mentioned localized structures are described by their thickness, which is shown to be proportional to the spatially damped oscillations period of the kink. The kink states have played a fundamental role to understand the localized synchronized states. In the next section, we shall study the transition from motionless to moving kink states, which is mediated by a non-variational Ising–Bloch transition

### 5. Non-variational Ising–Bloch transition

Bistable systems can exhibit domain walls connecting two homogeneous states. The features and dynamics of such domain walls have attracted attention across many fields of science. When one considers a bistable system with discrete symmetry – for instance reflection symmetry – the domain walls connecting such states are generically at rest because both states are “energetically” equivalents. However, under spontaneous symmetry-breaking, these fronts begin to propagate till they reach a constant asymptotic speed. This universal phenomenon of transition between stationary and propagating fronts connecting two equivalent states is usually denominated non-variational or non-equilibrium Ising–Bloch transition [53]. The stationary and moving domain walls, respectively, are usually denominated Ising and Bloch type walls in analogy to a magnetic transition [46]. Fig. 10 shows the typical observed propagative domain wall and the

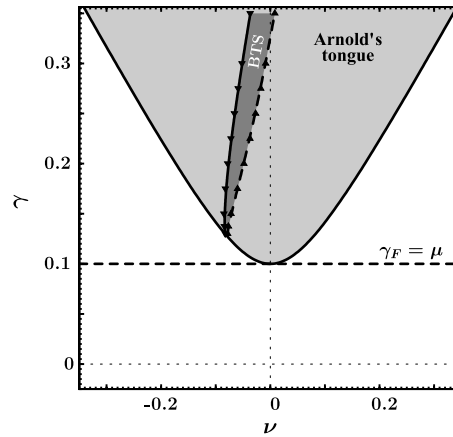


**Fig. 11.** Bifurcation diagram of the amended amplitude equation (Eq. (19)). The gray and dark gray areas stand for Arnold's tongue and the region of moving walls or Bloch type solution (BTS). The dashed and solid lines represent the non-variational Ising–Bloch transition and the spatial instability of the uniform non-null states. The parameters are:  $H_0 = 0.05$ ,  $\beta = 20.00$ ,  $\alpha = 0.01$  which correspond to  $\mu \simeq 0.10$ ,  $\omega_0 \simeq 1.00$ ,  $\alpha' \sim \delta \simeq 2.00$ ,  $\Gamma = 0.40$ ,  $d = 5 \times 10^{-4}$  and  $c = 0.40$ .

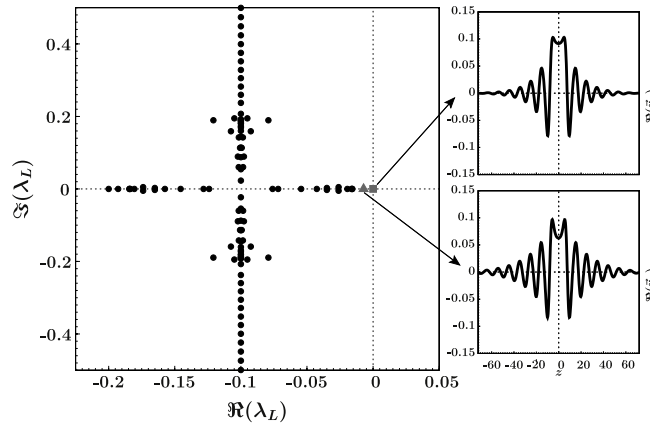


**Fig. 12.** Spectrum of linear operator  $\mathcal{L}$  which characterizes the linear stability of the Ising type wall of the model (19) with  $\gamma = 0.6$  and  $\nu = -0.06$ . The other parameters are the same used in Fig. 11. The inset figures are the real part of the eigenfunctions of the respective critical modes.

spatio-temporal dynamics exhibited by this state. Notice that this solution is asymmetric. Inside Arnold's tongue, we have characterized numerically the region where the Bloch type solutions (BTS) are displayed. This region is depicted in Fig. 11, where the dashed and solid lines represent the non-variational Ising–Bloch transition and the spatial instability of the uniform nonzero states. These states support the domain walls. Hence, to the left side region of BTS surface, the system does not exhibit domain walls.

To understand the mechanism of the non-equilibrium Ising–Bloch transition, we analyze the stability properties of the Ising type wall, that is, we shall compute the spectrum – set of eigenvalues – of the linear operator (which is denominated by  $\mathcal{L}(x)$ ) that describes the dynamics of small perturbations around the Ising type wall close to the Ising–Bloch transition. The lack of an analytical expression for the Ising type wall only allows us to compute numerically the spectrum, and their respective eigenfunctions. For the sake of simplicity, let us consider the following notation for the field  $A$ :

$$A(x, t) \equiv |A(x, t)\rangle,$$

which will allow us to write a compact expression for the front speed.

The typical spectrum of the Ising type wall observed close to the transition is shown in Fig. 12. Due to the translation invariance symmetry,  $x \rightarrow x + x_0$ , the spectrum always has an eigenvalue at the origin of the complex plane and the respective eigenfunction is known as its Goldstone mode. The upper inset on Fig. 12 depicts this mode. This mode characterizes the fact that an infinitesimal spatial translation of the Ising type wall is also a solution. Close to the transition, we have observed that there is an eigenvalue with zero imaginary and negative real part which moves to the origin of the complex plane. This eigenvalue and its respective eigenfunction are also depicted in Fig. 12 by a triangle and shown in the lower inset. Note that this eigenfunction is an asymmetric function with respect to the spatial center–core of the kink. At the transition this eigenvalue collides with the eigenvalue related to the Goldstone mode at the origin of the complex plane.

Subsequently, the mechanism of the Ising–Bloch transition is that an asymmetric spatial mode becomes unstable, namely, the system exhibits a spontaneous symmetry-breaking [46]. This transition is characterized by two critical modes, the asymmetric and the symmetric Goldstone modes, and these modes are related to the chirality and wall speed, respectively. The mathematical formulation reads

$$\mathcal{L} |A_{as}(x - P)\rangle = |\partial_z A_{Ising}(x - P)\rangle \quad (23a)$$

$$\mathcal{L}^2 |A_{as}(x - P)\rangle = 0 \quad (23b)$$

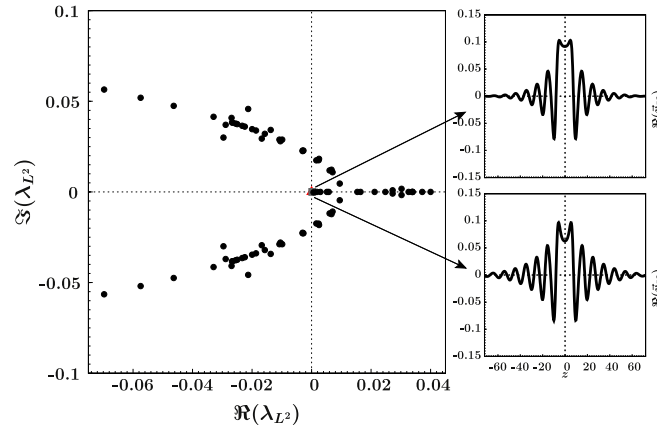


**Fig. 13.** Spectrum of the square of linear operator ( $\mathcal{L}^\varepsilon$ ) of Eq. (19), for the same parameters used in Fig. 12. The inset figures are the real part of the eigenfunctions of the respective critical modes.

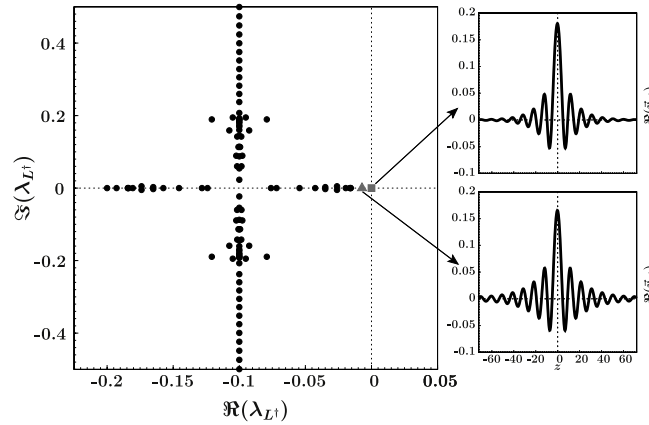


**Fig. 14.** Spectrum of the operator ( $\mathcal{L}^\dagger$ ) of Eq. (19) for the same parameters used in Fig. 12. The inset figures are the real part of the eigenfunctions of the respective critical modes.

where  $|A_{\text{Ising}}(x - P)\rangle$  is the Ising type solution, which is known only numerically,  $P$  stands for the position of the core of the Ising type wall, that is  $|A_{\text{Ising}}(0)\rangle = 0$ ;  $|A_{\text{as}}(x - P)\rangle$  is the critical asymmetric mode of the square of the linear operator  $\mathcal{L}$ , which is obtained using the standard Jordan construction Eqs. ((23)). Introducing the Ansatz

$$|A(x, t)\rangle = |A_{\text{Ising}}(x - P(\varepsilon t))\rangle + \varepsilon \chi(\varepsilon t) |A_{\text{as}}(x - P(\varepsilon t))\rangle + |W(x, P, \chi)\rangle, \quad (24)$$

where  $\chi(t)$  accounts for the amplitude of the asymmetric part (chirality),  $|W\rangle$  is a small complex correction ( $|W| \ll 1$ ) whose temporal dependence is implicit through the variable  $\{P, \chi\}$  and  $\varepsilon$  is an arbitrary small scale ( $\varepsilon \ll 1$ ) which is of the order of the square of the bifurcation parameter of the transition. Fig. 13 shows the two eigenfunctions of the operator  $\mathcal{L}^2$  associated with the zero eigenvalue, the lower inset shows  $|A_{\text{as}}\rangle$ , confirming the Jordan construction.

Notice that the above Ansatz (24) is based on the standard parameters variation method. Replacing this Ansatz in the amended amplitude equation (Eq. (19)) and linearizing in  $|W\rangle$  we obtain formally

$$-\varepsilon \dot{P} |\partial_z A_{\text{Ising}}(z)\rangle + \varepsilon^2 \dot{\chi} |A_{\text{as}}(z)\rangle = \mathcal{L} |W\rangle + |H(\chi, z, \varepsilon)\rangle, \quad (25)$$

where  $z \equiv x - P(\varepsilon t)$  is an auxiliary variable, the upper dot means temporal derivative in the slow time scale and  $H$  is a complex function. As result of spatial reflection symmetry ( $z \rightarrow -z$ ) and spatial invariance the function  $H$  is an odd function of chirality and is independent of  $P$ , this implies that this function has the form

$$|H(\chi, z, \varepsilon)\rangle = \varepsilon \chi |H_1(z)\rangle + \varepsilon^3 \chi^3 |H_3(z)\rangle + \dots$$

Introducing the Hilbert inner product

$$\langle f | g \rangle \equiv \int_{-\infty}^{\infty} f \bar{g} dx,$$

the linear operator  $\mathcal{L}$  is not self-adjoint ( $\mathcal{L} \neq \mathcal{L}^\dagger$ ). In order to solve Eq. (25) we must characterize the kernel of the adjoint  $\mathcal{L}^\dagger$  of the operator  $\mathcal{L}$ . Numerically, we can compute the eigenvalues and eigenfunctions of the  $\mathcal{L}^\dagger$ . Fig. 14 shows the spectrum and the eigenfunctions of the critical modes of  $\mathcal{L}^\dagger$ . The only element of the kernel of  $\mathcal{L}^\dagger$  is  $|A_+\rangle$ , which is illustrated in the upper inset of Fig. 14 for a given set of parameters. Then using this eigenfunction (Fredholm alternative), one obtains the following solvability condition up to order  $\varepsilon$ :

$$\dot{P} = \frac{\langle A_+(z) | H_1(z) \rangle}{\langle A_+(z) | \partial_z A_{\text{Ising}}(z) \rangle} \chi.$$

To obtain an equation for the chirality, we apply the linear operator  $\mathcal{L}$  to Eq. (25)

$$\varepsilon^2 \dot{\chi} \mathcal{L} |A_{as}(z)\rangle = \mathcal{L}^2 |W\rangle + \mathcal{L}H(\chi, z, \varepsilon),$$

where by definition  $\mathcal{L} |A_{as}(z)\rangle = |\partial_z A_{\text{Ising}}(z)\rangle$  (Jordan base). Thus, we can again apply the solvability condition and obtain

$$\dot{\chi} = \frac{\langle A_+(z) | \mathcal{L}H_1(z) \rangle}{\varepsilon \langle A_+(z) | \partial_z A_{\text{Ising}}(z) \rangle} \chi + \varepsilon \frac{\langle A_+(z) | \mathcal{L}H_3(z) \rangle}{\langle A_+(z) | \partial_z A_{\text{Ising}}(z) \rangle} \chi^3,$$

where the first term on the right-hand side is proportional to the bifurcation parameter of the transition, that is, this coefficient is zero at the transition. Scaling

$$\chi = \sqrt{-\varepsilon \frac{\langle A_+(z) | \partial_z A_{\text{Ising}}(z) \rangle}{\langle A_+(z) | \mathcal{L}H_3(z) \rangle}} \chi',$$

and introducing the constant

$$c \equiv \frac{\langle A_+(z) | H_1(z) \rangle}{\langle A_+(z) | \partial_z A_{\text{Ising}}(z) \rangle} \sqrt{-\varepsilon \frac{\langle A_+(z) | \partial_z A_{\text{Ising}}(z) \rangle}{\langle A_+(z) | \mathcal{L}H_3(z) \rangle}},$$

$$\eta \equiv \frac{\langle A_+(z) | \mathcal{L}H_1(z) \rangle}{\varepsilon \langle A_+(z) | \partial_z A_{\text{Ising}}(z) \rangle},$$

one obtains the following set of equations for the critical modes

$$\dot{P} = c \chi',$$

$$\dot{\chi}' = \eta \chi' - \chi'^3. \tag{26}$$

The coefficients  $\{c, \eta\}$  can be computed numerically for the specific values of parameters. Hence, the wall speed ( $\dot{P} \equiv v$ ) is proportional to the chirality and the chirality exhibits a stationary pitchfork bifurcation at  $\eta = 0$ . Subsequently, for negative  $\eta$ , an initial asymmetric wall moves during a transient and then it becomes motionless. In contrast, for positive  $\eta$ , an initial asymmetric wall moves during a transient and becomes a moving domain wall with well defined velocity  $\dot{P} = v = c \sqrt{\eta}$ . Depending on the form of the initial condition the wall propagates to the left or to the right. Using the above equation we can obtain the following equation for the speed

$$\dot{v} = \eta v - \frac{v^3}{c^2}. \tag{27}$$

This equation has been obtained in reaction–diffusion models [66], and nonlinear optics [53]. However, it is important to note that the non-variational Ising–Bloch transition is characterized by the two order parameters  $\{P, \chi'\}$ . The model (26) describes a stationary bifurcation with two modes and one eigenfunction, which is denoted in Arnold's notation as the  $(0)^2$  instability [63]. In the special case of  $c = 0$ —there is an stationary bifurcation characterized by two different eigenfunctions – the system exhibits a Ising–Bloch transition, however the Bloch type walls are motionless. This is the classical case observed in magnetic systems, where the transition is in equilibrium [46].

## 6. Concluding remarks

We have shown that an easy-plane ferromagnetic classical spin chain is equivalent to a nonlinear oscillator. A novel approach to study the evolution of this oscillator, the amended amplitude equation, allows us to characterize the synchronized precession states inside Arnold's tongue close to the parametric resonance. Indeed the standard approximation of such a quasi-reversible system – the Parametrically Driven and Damped Nonlinear Schrödinger (PDNLS) equation – turns out to be structurally unstable, through the linear stability analysis of the uniform state that represents the synchronized precession. Hence, this approach fails to describe the synchronized precession states observed in the original system. Our amended model accounts for the behavior of the aforementioned states and allows us to give a justification for the existence of an extended family of particle type solutions in a forced magnetic wire.

In fact, due to the existence of a parity symmetry in the system, there are two synchronized precession states which are out of phase. As long as these states are stable, from a dynamical system's point of view, one can have an infinite family of trajectories connecting them asymptotically. The trajectories connecting different states are the kink or the anti-kink solutions. These solutions are important since all the other localized states can be built up by the superposition of them. The main characteristic of these localized states (their size) is shown to be a multiple of the characteristic length of the spatially damped oscillations appearing in the kink states. As the kink solution connects two equivalent states, then we expect to observe a motionless domain wall between the states. However, due to the non-variational nature of model (19) and the spontaneous spatial symmetry-breaking, this amended model exhibits a non-variational Ising–Bloch transition. Thus, this system exhibits moving domain walls. Close to this transition, we have derived a simple set of ordinary differential equations for the position and chirality – amplitude of the asymmetric mode – of the domain walls. This set of equations allows us to understand in a simple manner the non-variational Ising–Bloch transition.

## Acknowledgements

The authors thank C. Falcón and E. Tirapegui for the fruitful comments. The simulation software *DimX*, developed at INLN (France), has been used for the numerical simulations presented in this paper. The authors thank the support of ring program ACT15 of the *Programa Bicentenario* of the Chilean Government. M.G.C. acknowledges the financial support of FONDECYT project 1090045, and FONDAP grant 11980002. D.L. thanks the partial support of the ring program ACT24 of the *Programa Bicentenario* of the Chilean Government, Millennium Science Nucleus P06 – 022 – F, FONDECYT 11080229 and *Convenio de desempeño* UTA MECESUP-2. S.C. thanks the financial support of FONDECYT 3080041.

**Appendix. Amended amplitude equation for the magnetization components**

Let us start by the Landau–Lifshitz–Gilbert equation given as follows:

$$\partial_t \mathbf{M} = \mathbf{M} \times [\mathbf{M}_{zz} - \beta (\mathbf{M} \cdot \hat{z}) \hat{z} + \mathbf{H}_e - \alpha \partial_t \mathbf{M}]. \quad (\text{A.1})$$

Since we have  $\mathbf{M} \equiv (M_x, M_y, M_z)$  and  $\mathbf{H}_e = H(t)\hat{x}$  these equations read

$$\dot{M}_x = M_y \partial_z^2 M_z - M_z \partial_z^2 M_y - \beta M_y M_z + \alpha (\partial_z^2 M_x + H(t)) - \alpha M_x (M_x \partial_z^2 M_x + M_y \partial_z^2 M_y + M_z \partial_z^2 M_z + M_x H(t) - \beta M_z^2), \quad (\text{A.2})$$

$$\dot{M}_y = M_z \partial_z^2 M_x - M_x \partial_z^2 M_z + M_z H(t) + \beta M_x M_z + \alpha \partial_z^2 M_y - \alpha M_y (M_x \partial_z^2 M_x + M_y \partial_z^2 M_y + M_z \partial_z^2 M_z + M_x H(t) - \beta M_z^2), \quad (\text{A.3})$$

$$\dot{M}_z = M_x \partial_z^2 M_y - M_y \partial_z^2 M_x - M_y H(t) + \alpha (\partial_z^2 M_z - \beta M_z) - \alpha M_z (M_x \partial_z^2 M_x + M_x H(t) + M_y \partial_z^2 M_y + M_z \partial_z^2 M_z - \beta M_z^2). \quad (\text{A.4})$$

At equilibrium, the magnetization is parallel to the applied external field, that is  $\mathbf{M}(z, t) = (1, 0, 0)$ . Therefore, assuming a small deviation for the precession states we can write

$$\mathbf{M}(z, t) = \begin{pmatrix} \sqrt{1 - (M_x(z, t)^2 + M_y(z, t)^2)} \\ M_x(z, t) \\ M_z(z, t) \end{pmatrix} \sim \begin{pmatrix} 1 - (M_x^2 + M_y^2)/2 + \dots \\ M_x \\ M_z \end{pmatrix}.$$

Introducing this development in (A.3) and (A.4) and neglecting the nonlinear terms with spatial derivatives and damping, the precession dynamics is modeled by

$$\dot{M}_y = (\beta + H) M_z - \alpha H M_y - \partial_z^2 M_z - \beta \frac{M_y^2 + M_z^2}{2} M_z, \quad (\text{A.5})$$

$$\dot{M}_z = -H M_y - \alpha (\beta + H) M_z + \partial_z^2 M_y. \quad (\text{A.6})$$

Deriving (A.6) with respect to time and replacing the term  $\dot{M}_z$  in Eq. (A.5), we obtain

$$\begin{aligned} \ddot{M}_z = & -\dot{H} M_y - H \left[ (\beta + H) M_z - \alpha H M_y - \partial_z^2 M_z - \beta \frac{M_y^2 + M_z^2}{2} M_z \right] - \alpha \dot{H} M_z \\ & - \alpha (\beta + H) \dot{M}_z + \partial_z^2 \left[ (\beta + H) M_z - \alpha H M_y - \partial_z^2 M_z - \beta \frac{M_y^2 + M_z^2}{2} M_z \right]. \end{aligned} \quad (\text{A.7})$$

Keeping in mind that  $\partial_z^4 M_z \ll \partial_z^2 M_z \ll \partial_z M_z$ ,  $\alpha \sim \varepsilon \ll 1$ ,  $M_z \sim \sqrt{\varepsilon} \ll 1$ , at the leading order in  $\varepsilon$ , (A.7) reads

$$\begin{aligned} \ddot{M}_z = & -\dot{H} M_y - H \left[ (\beta + H) M_z - \frac{\beta}{2} (M_y^2 + M_z^2) M_z - \partial_z^2 M_z - \alpha M_y H \right] - \alpha \dot{H} M_z \\ & - \alpha (\beta + H) \dot{M}_z + (\beta + H) \partial_z^2 M_z - \alpha H \partial_z^2 M_y. \end{aligned} \quad (\text{A.8})$$

Using the slowly varying envelope approximation, it can deduced from (A.6) that  $M_y$  and  $M_z$  can be related by:

$$M_y \approx -\frac{1}{H} \dot{M}_z - \alpha \frac{\beta + H}{H} M_z. \quad (\text{A.9})$$

Defining  $H(t) = H_0 - h_1(t)$ , with  $|h_1(t)| \sim \varepsilon \ll H_0$ , we obtain

$$\frac{1}{H(t)} \approx \frac{1}{H_0} + \frac{h_1(t)}{H_0^2}. \quad (\text{A.10})$$

Then Eq. (A.8) reads

$$\begin{aligned} \ddot{M}_z = & -\frac{1}{H_0} \dot{h}_1 \dot{M}_z - \frac{\alpha \beta}{H_0} \dot{h}_1 M_z - H_0 (\beta + H_0) M_z - (\beta + 2H_0) h_1 M_z + (\beta + 2H_0) \partial_z^2 M_z \\ & - \alpha (\beta + 2H_0) \dot{M}_z - h_1^2 M_z - \alpha (\alpha H_0 (\beta + H_0) M_z - h_1 \dot{M}_z) + \alpha \partial_z^2 \dot{M}_z + \alpha^2 (\beta + 2H_0) \partial_z^2 M_z \\ & + \frac{\beta}{2H_0} \left( 1 + \frac{h_1}{H_0} \right) [\dot{M}_z^2 + H_0 M_z^2 + 2(-H_0 h_1 M_z^2 + \alpha (\beta + H_0) \dot{M}_z M_z)] M_z. \end{aligned}$$

At the leading order we have

$$\ddot{M}_z = -H_0 (\beta + H_0^2) M_z + \frac{\beta}{2H_0} (M_z^2 + H_0 M_z^2) M_z + (\beta + 2H_0) \partial_z^2 M_z - (\beta + 2H_0) h_1 M_z - \frac{1}{H_0} \dot{h}_1 \dot{M}_z - \alpha (\beta + 2H_0) \dot{M}_z. \quad (\text{A.11})$$

This equation is the analogue of a nonlinear forced and damped oscillator with natural frequency  $\omega_0 = \sqrt{H_0 (\beta + H_0)}$ . Now we consider a parametric forcing ( $h_1(t) = h \sin[2(\omega_0 + \nu)t]$ ,  $\nu \sim \varepsilon \ll 1$ ), and we write the solutions in the form  $M_z(z, t) = C(Z, T)e^{i\omega_0 t} + \bar{C}(Z, T)e^{-i\omega_0 t} + \dots$ , where  $Z$  and  $T$  are the slowly variables. The amplitude of  $M_z(z, t)$  satisfies

$$\partial_T C = -i\nu C - i \frac{\beta (\omega_0^2 + 3H_0^2)}{4\omega_0 H_0} |C|^2 C - i \frac{\beta + 2H_0}{2\omega_0} \partial_Z^2 C - \alpha \frac{\beta + 2H_0}{2} C + h \frac{\beta}{4\omega_0} \bar{C}. \quad (\text{A.12})$$

We have shown (see Section 3.2) that inside Arnold's tongue (A.12) fails to describe the spatial homogeneous synchronized precession state. That is Eq. (A.12) must be corrected by the higher order term ( $O(\varepsilon^{\frac{5}{2}})$ ) of (A.10). Thus

$$\begin{aligned}\frac{\alpha\beta}{H_0}\dot{h}_1\dot{M}_z &= \alpha h \frac{\omega_0\beta}{H_0}\bar{C}e^{2ivt}e^{i\omega_0t} + c.c., \\ \alpha\partial_z^2\dot{M}_z &= i\alpha\omega_0\partial_z^2C e^{i\omega_0t} + c.c., \\ \alpha(\alpha H_0(\beta + H_0)M_z + h_1\dot{M}_z) + h_1^2M_z &= \left(\alpha^2\omega_0^2 + \frac{h^2}{2}\right)C e^{i\omega_0t} - \alpha h \frac{\omega_0}{2}\bar{C}e^{2ivt}e^{i\omega_0t} + c.c., \\ h_1\frac{\beta}{2H_0^2}(H_0^2M_z^2 - \dot{M}_z^2)M_z &= \frac{ih\beta}{4H_0^2}\left[(\omega_0^2 - 3H_0^2)|C|^2\bar{C}e^{2ivt} + (\omega_0^2 + H_0^2)C^3e^{-2ivt}\right]e^{i\omega_0t} + c.c., \\ \alpha\frac{\beta\omega_0^2}{H_0^2}\dot{M}_zM_z^2 &= i\alpha\frac{\beta\omega_0^3}{H_0^2}|C|^2C e^{i\omega_0t} + c.c.\end{aligned}$$

Then the amended equation reads

$$\begin{aligned}\partial_t C &= -ivC - i\frac{\beta(\omega_0^2 + 3H_0^2)}{4\omega_0H_0}|C|^2C - i\frac{\beta + 2H_0}{2\omega_0}\partial_z^2C - \alpha\frac{\beta + 2H_0}{2}C - h\frac{\beta}{4\omega_0}\bar{C} \\ &\quad + \frac{\alpha}{2}\partial_z^2C - i\frac{\alpha h}{4H_0}(H_0 + 2\beta)\bar{C} + \frac{h\beta}{8\omega_0H_0^2}\left[(\omega_0^2 - 3H_0^2)|C|^2\bar{C} + (\omega_0^2 + H_0^2)C^3\right] + \alpha\frac{\beta\omega_0^2}{2H_0^2}|C|^2C.\end{aligned}$$

Introducing

$$C = 2\sqrt{\frac{\omega_0H_0}{\beta(\omega_0^2 + 3H_0^2)}}A, \quad (\text{A.13a})$$

$$Z = \sqrt{\frac{\beta + 2H_0}{2\omega_0}}\zeta, \quad (\text{A.13b})$$

$$\mu = \alpha\frac{\beta + 2H_0}{2}, \quad (\text{A.13c})$$

$$\gamma = h\frac{\beta}{4\omega_0}, \quad (\text{A.13d})$$

$$d = \frac{\omega_0\alpha}{\beta + 2H_0}, \quad (\text{A.13e})$$

$$\Gamma = \frac{2\alpha\omega_0^2}{\beta H_0^2}, \quad (\text{A.13f})$$

$$\alpha' = 2\omega_0\frac{3H_0^2 - \omega_0^2}{\beta H_0(\omega_0^2 + 3H_0^2)}, \quad (\text{A.13g})$$

$$\delta = -2\omega_0\frac{H_0^2 + \omega_0^2}{\beta H_0(\omega_0^2 + 3H_0^2)}, \quad (\text{A.13h})$$

$$c = \frac{2\alpha\omega_0^2}{H_0(\omega_0^2 + 3H_0^2)}, \quad (\text{A.13i})$$

we finally obtain:

$$\partial_t A = -ivA - (i - c)|A|^2A - i\partial_z^2A - \mu A + \gamma(1 + i\Gamma)\bar{A} - \gamma\alpha'|A|^2\bar{A} - \gamma\delta A^3, \quad (\text{A.13j})$$

where the natural frequency is corrected by the expression:

$$\Omega_0^2 = \left(1 - \alpha^2 - \frac{h^2}{2\omega_0^2}\right)\omega_0^2. \quad (\text{A.14})$$

## References

- [1] H.A. Eschenfelder, *Magnetic Bubble Technology*, Springer Verlag, Berlin, 1981.
- [2] S. Pirkl, P. Ribiere, P. Oswald, *Liq. Cryst.* 13 (1993) 413.
- [3] Y.A. Astrov, Y.A. Logvin, *Phys. Rev. Lett.* 79 (1997) 2983.
- [4] K.-jin Lee, W.D. McCormick, J.E. Pearson, H.L. Swinney, *Nature* 369 (1994) 215.
- [5] W.S. Edwards, S. Fauve, *J. Fluid Mech.* 278 (1994) 123.
- [6] P.B. Umbanhowar, F. Melo, H.L. Swinney, *Nature* 382 (1996) 793.
- [7] M.G. Clerc, P. Cordero, J. Dunstan, K. Huff, N. Mujica, D. Risso, G. Varas, *Nat. Phys.* 4 (2008) 249.
- [8] R. Heinrichs, G. Ahlers, D.S. Cannell, *Phys. Rev. A* 35 (1987) R2761.
- [9] P. Kolodner, D. Bensimon, C.M. Surko, *Phys. Rev. Lett.* 60 (1988) 1723.
- [10] D.W. McLaughlin, J.V. Moloney, A.C. Newell, *Phys. Rev. Lett.* 51 (1983) 75.

- [11] R. Neubecker, G.L. Oppo, B. Thuring, T. Tschudi, *Phys. Rev. A* 52 (1995) 791.
- [12] B. Schpers, M. Feldmann, T. Ackemann, W. Lange, *Phys. Rev. Lett.* 85 (2000) 748.
- [13] G. Nicolis, I. Prigogine, *Self-organization in Non Equilibrium systems*, Wiley & sons, New York, 1977.
- [14] M.C. Cross, P.C. Hohenberg, *Rev. Modern. Phys.* 65 (1993) 851.
- [15] M. Faraday, *Phil. Trans. R. Soc.* 121 (1831) 299.
- [16] J.W. Miles, *J. Fluid Mech.* 148 (1984) 451;  
W. Zhang, J. Viñals, *Phys. Rev. Lett.* 74 (1995) 690;  
X. Wang, R. Wei, *Phys. Rev. E* 57 (1998) 2405.
- [17] J. Wu, R. Keolian, I. Rudnick, *Phys. Rev. Lett.* 52 (1984) 1421.
- [18] J.W. Miles, *J. Fluid Mech.* 148 (1984) 451.
- [19] C. Elphick, E. Meron, *Phys. Rev. A* 40 (1989) 3226.
- [20] X. Xang, R. Wei, *Phys. Lett.* 192 (1994) 1.
- [21] Xinlong Wang, Rongjue Wei, *Phys. Rev. Lett.* 78 (1997) 2744.
- [22] Likun Zhang, Xinlong Wang, Zhiyong Tao, *Phys. Rev. E* 75 (2007) 036602.
- [23] I.V. Barashenkov, M.M. Bogdan, V.I. Korobov, *Europhys. Lett.* 15 (1991) 113.
- [24] S. Gluzman, *Phys. Rev. B* 50 (1994) 13 809.
- [25] A. Mecozzi, W.L. Kath, P. Kumar, C.G. Goedde, *Opt. Lett.* 19 (1994) 2050;  
C.G. Goedde, W.L. Kath, P. Kumar, *Opt. Lett.* 19 (1994) 2077.
- [26] S. Longhi, *Opt. Lett.* 20 (1995) 695;  
S. Longhi, A. Geraci, *Appl. Phys. Lett.* 67 (1995) 3060.
- [27] S. Longhi, *Phys. Rev. E* 53 (1996) 5520.
- [28] A. Jotes, R. Ribotta, *Phys. Rev. Lett.* 60 (1988) 2164.
- [29] S. Barland, et al., *Nature* 419 (2002) 699.
- [30] B. Denardo, et al., *Phys. Rev. Lett.* 68 (1992) 1730.
- [31] J.N. Kutz, et al., *Opt. Lett.* 18 (1993) 802.
- [32] S. Longhi, *Phys. Rev. E* 53 (1996) 5520.
- [33] I.V. Barashenkov, M.M. Bogdan, V.I. Korobov, *Europhys. Lett.* 15 (1991) 113.
- [34] N.V. Alexeeva, I.V. Barashenkov, G.P. Tsironis, *Phys. Rev. Lett.* 84 (2000) 3053.
- [35] Kapitula, Sandstede, *Physica D* 124 (1998) 58.
- [36] Promislow, Kutz, *Nonlinearity* 13 (2000) 675.
- [37] Chang, Promislow, *Nonlinearity* 20 (2007) 743.
- [38] P. Couillet, *Internat. J. Bif. Chaos* 12 (2002) 245.
- [39] M.G. Clerc, S. Coulibaly, D. Laroze, *Phys. Rev. E* 77 (2008) 056209.
- [40] Wim van Saarloos, *Phys. Rep.* 386 (2003) 29.
- [41] J.D. Murray, *Mathematical Biology*, Springer-Verlag, Berlin, 1989.
- [42] S. Residori, A. Petrossian, T. Nagaya, C. Riera, M.G. Clerc, *Physica D* 199 (2004) 149.
- [43] M.G. Clerc, T. Nagaya, A. Petrossian, S. Residori, C. Riera, *Eur. Phys. J. D* 28 (2004) 435.
- [44] W.K. Burton, N. Cabrera, F.C. Frank, *Phil. Trans. Roy. Soc. London A* 243 (1951) 299.
- [45] R.E. Goldstein, G.H. Gunaratne, I. Gil, P. Couillet, *Phys. Rev. A* 43 (1991) 6700.
- [46] P. Couillet, J. Lega, B. Houchmanzadeh, J. Lajzerowicz, *Phys. Rev. Lett.* 65 (1990) 1352.
- [47] L.N. Bulaevsky, V.L. Ginzburg, *Sov. Phys. JETP* 18 (1964) 530.
- [48] J.M. Gilli, M. Morabito, T. Frisch, *J. Phys. II* 4 (1994) 314.
- [49] D. Haim, G. Li, Q. Ouyang, W.D. McCormick, H.L. Swinney, A. Hagberg, E. Meron, *Phys. Rev. Lett.* 77 (1996) 190.
- [50] R. Graham, *Tel. Phys. Rev. A* 33 (1986) 1322.
- [51] O. Descalzi, E. Tirapegui, *J. Statist. Phys.* 57 (1989) 993.
- [52] F. Barra, O. Descalzi, E. Tirapegui, *Phys. Lett. A* 221 (1996) 193.
- [53] D. Michaelis, U. Peschel, F. Lederer, D.V. Skryabin, W.J. Firth, *Phys. Rev. E* 63 (2001) 066602.
- [54] Kittel Charles, *Rev. Modern. Phys.* 21 (1949) 541.
- [55] V. Zharnitsky, I. Mitkov, Mark Levi, *Phys. Rev. B* 57 (1998) 5033.
- [56] H.J. Mikeska, *J. Phys. C* 11 (1978) L29.
- [57] A.M. Kosevich, B.A. Ivanov, A.S. Kovalev, *Phys. Rep.* 194 (1990) 117.
- [58] M. Clerc, P. Couillet, E. Tirapegui, *Phys. Rev. Lett.* 83 (1999) 3820; *Internat. J. Bif. Chaos* 11 (2001) 591; *Opt. Commun.* 166 (1999) 159; *Phys. Lett. A* 287 (2001) 198; *Prog. Theor. Phys. Suppl.* 139 (2000) 337.
- [59] L.D. Landau, E.M. Lifchitz, *Mechanics*, Pergamon Press, Burligton, 2003.
- [60] L. Pismen, *Patterns and Interfaces in Dissipative Dynamics*, Springer Verlag, 2006.
- [61] Alan C. Newell, *Solitons in Mathematics and Physics*, SIAM, Philadelphia, 1985.
- [62] P. Couillet, T. Frisch, G. Sonnino, *Phys. Rev. E* 49 (1994) 2087.
- [63] V.I. Arnold, *Geometrical Methods in the Theory of Ordinary Differential Equations*, Springer-Verlag, New York, 1983.
- [64] M.G. Clerc, D. Escaff, V.M. Kenkre, *Phys. Rev. E* 72 (2005) 056217. and the references therein.
- [65] M.G. Clerc, C. Falcon, *Physica A* 356 (2005) 48.
- [66] C. Elphick, A. Hagberg, Meron, *Phys. Rev. E* 51 (1995) 3052.